Proceedings of ERAD 2006

# A C-band fully self-consistent methodology to correct attenuation and differential attenuation

**Eugenio Gorgucci and Luca Baldini**

Institute of Atmospheric Sciences and Climate – CNR, Roma (Italy).

## 1 Introduction

Although is not a major error source at C-band, attenuation may degrade the radar measurement to a considerable degree in situations like a precipitation event in the radar shadow of a strong convective cell, or may affect precipitation accumulation estimates at distances far from the radar site. For C-band radars, attenuation can be corrected using different methods depending on the type of measurements involved. The early attenuation correction procedures were based on iterative approaches without bounds and were unstable (Aydin et al. 1989). Studying the relation between differential phase ($\Phi_{dp}$) and cumulative attenuation as well as differential attenuation at S-, C-, and X-band frequencies, Bringi et al. (1990) explored a simple attenuation correction procedure based on linear relations between $\Phi_{dp}$ and cumulative path attenuation and differential attenuation. More recently, the cumulative attenuation estimate provided by cumulative differential phase was used as a constraint to obtain the profile of specific attenuation have been proposed (Testud et al., 2000). In the latter two techniques, a constant coefficient is used to convert $\Phi_{dp}$ to cumulative attenuation. Alternatives techniques, employing empirical adjustment to the conversion coefficient, were also suggested (Smyth and Illingworth 1999, Bringi et al. 2001). One of the advantages of polarimetric radar measurements in rain is their internal self-consistency. The self-consistency principle (Scarchilli et al. 1996) takes advantage of the synergy among the radar measurements, namely reflectivity factor ($Z_h$), differential reflectivity ($Z_{dr}$), and specific differential propagation phase ($K_{dp}$) and has been proven as a powerful tool in several applications. Gorgucci et al. (2006) applied it in a methododology for attenuation and differential attenuation correction at X-band. This paper presents an advance of this methodology and evaluates it both using C-band profiles generated from S-band radar measurements collected by the NCAR S-Pol radar and C-band radar data collected by the Polar 55C radar over the region of Rome region (Italy).

*Correspondence to:* Eugenio Gorgucci

e.gorgucci@isac.cnr.it

## 2 ATTENUATION CORRECTION ALGORITHMS BASED ON THE SELF-CONSISTENCY PRINCIPLE

For specific attenuation ($\alpha_h$), Bringi et al. (1990) introduced the parameterization of the form

$$\alpha_h = a_h K_{dp} \quad (\mathrm{dB\,km^{-1}}) \tag{1}$$

where $a_h$ depends on various factors such as DSD, mean raindrop shape, as well as temperature. A parameterization of the specific differential attenuation ($\alpha_d$) using a linear $\alpha_d$-$K_{dp}$ relationship was also proposed. However, it is not nearly as good as (1) at C-band. Different parameterizations of $\alpha_h$ and $\alpha_d$ using $Z_h$ and $Z_{dr}$ were studied (Gorgucci et al. 1998) as well as that relating $a_h$ and $\alpha_d$

$$\alpha_d = \varepsilon \alpha_h \quad (\mathrm{dB\,km^{-1}}) \tag{2}$$

Gorgucci et al. (2006) introduced parameterizations based on the self-consistency principle joining $Z_h$, $Z_{dr}$, $K_{dp}$, with $\alpha_h$ (or $\alpha_d$) of the form

$$\alpha_h\left(Z_h, Z_{dr}, K_{dp}\right) = a_h Z_h^{b_h} Z_{dr}^{c_h} K_{dp}^{d_h} \quad (\mathrm{dB\,km^{-1}}) \tag{3a}$$

$$\alpha_d\left(Z_h, Z_{dr}, K_{dp}\right) = a_d Z_h^{b_d} Z_{dr}^{c_d} K_{dp}^{d_d} \quad (\mathrm{dB\,km^{-1}}) \tag{3b}$$

Coefficients in (3) have a small variation with drop-shape model. The coefficients are computed as a mean fit of widely varying DSDs for raindrops following the Pruppacher and Beard (1970) model and for a temperature of 20 °C; canting angle is assumed as Gaussian distributed with zero mean and standard deviation of 10 degrees. The coefficients of (3a) are $a_h$=2.546×10$^{-5}$, $b_h$=0.776,$c_h$=-0.340, $d_h$=0.193, while those of (3b) are $a_d$=9.174×10$^{-6}$, $a_d$=0.674, $c_d$=0.804, $d_d$=0.380. The excellent behavior of these parameterizations is shown by

the small normalized bias (NB, -0.5% and -1.5% for $\alpha_h$ and $\alpha_d$, respectively) and normalized standard error (NSE, 11.3% and 28.2%, respectively). Similarly, the coefficient of (2) can be found to be 0.289. Fig 1. compares parameterizations of $\alpha_h$ highlighting the strong reduction of the spread achieved using (3a) with respect to (1).

These parameterizations cannot be directly used to estimate $\alpha_h$ and $\alpha_d$ due to both attenuation suffered by $Z_h$ and $Z_{dr}$ and to practical considerations in computing $K_{dp}$ (Gorgucci, 2000). To overcome these problems, (3) can be rearranged to express $K_{dp}$ in terms of $Z_h$, $Z_{dr}$, and $\alpha_h$ (or $\alpha_d$). Using the preliminary estimates $Z_h$, $Z_{dr}$, and $\alpha_h$ (or $\alpha_d$) obtained by means of differential phase constrained (DPC) method (Testud et al, 2000) and (2), two preliminary estimates of the reconstructed differential phase $\Phi_{dp}^{h}$ and $\Phi_{dp}^{d}$ are obtained, respectively from (3a) and (3b) and then compared against the corresponding measured profile. The differences $\Delta_h$ and $\Delta_d$, between the reconstructed and measured differential phase profiles can be minimized for $\alpha_h$ and $\alpha_d$ as

$$\min(\Delta_h) = \min\left\{\int_{r_0}^{r} \gamma_h \Phi_{dp}^{h}(s) - \left[\Phi_{dp}(s) - \Phi_{dp}(r_0)\right] ds\right\} \quad (4a)$$

$$\min(\Delta_d) = \min\left\{\int_{r_0}^{r} \gamma_d \Phi_{dp}^{d}(s) - \left[\Phi_{dp}(s) - \Phi_{dp}(r_0)\right] ds\right\} \quad (4b)$$

where $\gamma_h$ and $\gamma_d$ are multiplicative factors, yielding a modified $\tilde{\alpha}_h$ and $\tilde{\alpha}_d$ given by

$$\tilde{\alpha}_h = \gamma_h^{d_h}\, \alpha_h \quad (5a)$$

$$\tilde{\alpha}_d = \gamma_d^{d_d}\, \alpha_d \quad (5b)$$

In this way, for a given measured $\Phi_{dp}$ profile, $\alpha_h$ and $\alpha_d$ profiles estimated from a first guess will be scaled down or up. This concept is implemented as follows:

a) $\alpha_h$ and $\alpha_d$ profiles are obtained from DPC method and (2) and used to obtain corrected $Z_h$ and $Z_{dr}$ profiles;
b) Using (4a), $\gamma_h$ is obtained;
c) Utilizing $\gamma_h$, (5a) and (2) a differential attenuation profile is obtained and jointly used with $Z_h$, $Z_{dr}$ and $\Phi_{dp}$ profiles to obtain an estimation of $\gamma_d$ from (4b);
d) Making use of $\gamma_h$, $\gamma_d$, and (5), attenuation and differential attenuation profiles are obtained and used to correct $Z_h$, and $Z_{dr}$ profiles;
e) If the estimates $\gamma_h$ and $\gamma_d$ vary for more than 0.5 % with respect to the previous ones, the process is repeated from step b) to step e).

This iterative process converges fairly quickly, demonstrating the numerical stability of the procedure. This method (hereafter denoted as FSC) can be seen as a fully self-consistency chain joining $\Phi_{dp}$, $Z_h$, $Z_{dr}$, $\alpha_h$, and $\alpha_d$. Factors that can result in differences between the observed and estimated profiles of $\Phi_{dp}$ are the DSD dependence as well as the drop-shape model dependence. FSC will simultaneously optimize both the difference due to the drop-shape model as well as the DSD difference.

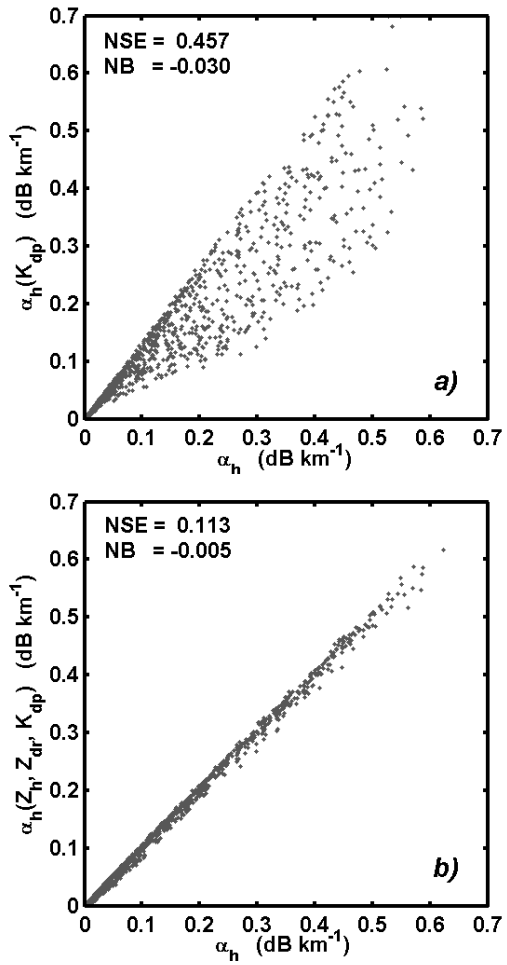


**Fig. 1.** Scatter plots between specific attenuation and its estimates obtained using parameterizations based on a) $K_{dp}$, and b) ($Z_h$, $Z_{dr}$, $K_{dp}$). The parameterizations are found for the PB drop-shape model.

The procedure described above is different from that applied to X-band by Gorgucci et al. (2006), hereafter referred as SC, where (4a) and (4b) were used independently to obtain separately corrected attenuation and differential attenuation profiles by iterative procedures.

## 3 Data sources

### 3.1 Polar 55C data

The Polar 55C data were collected at the CNR-ISAC atmospheric observatory in Rome, where the Polar 55C - a coherent C-band dual-polarized radar - has been operating since 2001 (Gorgucci et al., 2002), during a campaign conducted throughout the second semester of 2004. Measurements were obtained integrating 64 sample pairs of radar returns at h e v polarizations obtained with a pulse repetition time of 0.85 ms. The analysis has been performed taking 1560 profiles composed at least of 130 range bins 130 range bins at a distance of 75 m apart with differential phase increasing along the path greater than 6 degrees, carefully selected to avoid ground clutter, bright band and anomalous propagation effects, etc.

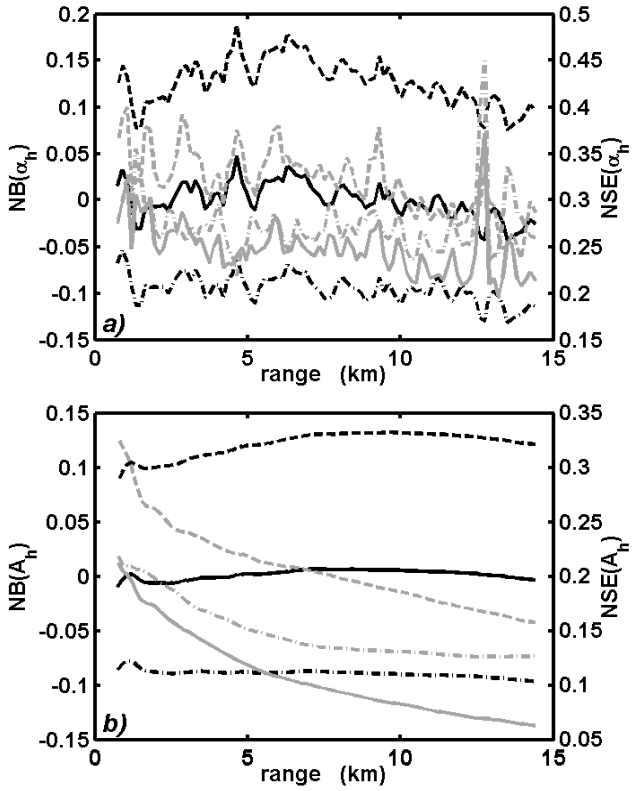


**Fig. 2.** NB (black) and NSE (grey) of a) specific attenuation and b) cumulative attenuation estimated by DPC (dashed), SC (dash-dot), FSC (solid).

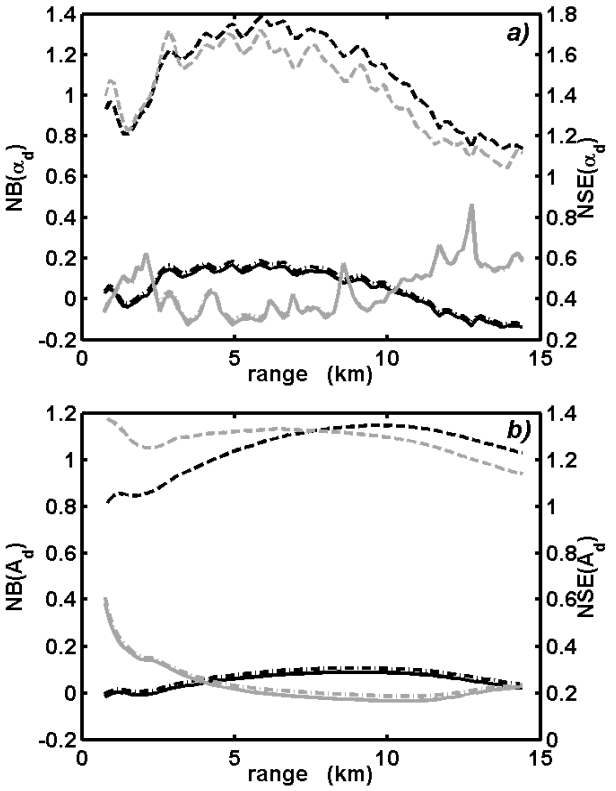


**Fig. 3.** NB (black) and NSE (grey) of a) specific differential attenuation and b) cumulative differential attenuation estimated by DPC (dashed), SC (dash-dot), FSC (solid).

### 3.2 Reconstructed C-Band Rain Profiles

S-band profiles used to reconstruct realistic C-band profiles were selected from data collected by the NCAR S-POL radar during two campaigns: i) TEFLUN-B (Central Florida, August 1 - September 30, 1998), an experiment in support of the Ground Validation segment of the TRMM; ii) Mesoscale Alpine Programme (MAP) during which S-POL was located at the southern end of the Lago Maggiore (Italy); the Intense Observation Period 02, (September 19-21, 1999) was considered. All 15-km rain paths (the range resolution was 150 m) with an increasing $\Phi_{dp}$ along the path greater than 6 degrees were chosen. C-band profiles were generated according to Chandrasekar et al. (2006). Since ($Z_h$, $Z_{dr}$, $K_{dp}$) triplets nearly lie on a three-dimensional surface when the drop-shape model is fixed (Scarchilli 1996), once $Z_h$ and $Z_{dr}$ are specified, the choice of possible $K_{dp}$ values falls in a narrow range. Therefore, for each ($Z_h$, $Z_{dr}$) pair of S-POL profiles, a search in a set of radar measurement simulated at S-band provides a possible choice of different DSDs that satisfy the observations. One DSD is randomly chosen to establish the corresponding C-band profiles. The Pruppacher and Beard (1970) drop-shape model is assumed. Random signal fluctuation and differential backscatter phase shift are also considered in the C-band reconstructed profiles.

## 4 Evaluation of the methodology

C-band range profiles generated from S-band observations are used first to compare the performance of DPC, SC, and FSC method. For brevity, only figures concerning MAP are presented. Figs. 2a and 2b report the assessment of attenuation and cumulative attenuation estimations obtained with DPC, SC and FSC methods weighted against the true. Fig. 2a shows normalized bias (black line) and normalized standard error (grey line) of specific attenuation estimates using the DPC (dashed line), SC (dash-dot line) and FSC (solid line) methods as a function of the rain path. The figure illustrates the very good performance of $\alpha_h$ estimation with FSC, which is characterized by a NB very close to zero and by the smaller NSE with averaged value of about 24%. Fig. 2b refers to the same parameters for cumulative attenuation estimates $A_h$. FSC performance is pointed out by a negligible NB and smaller NSE with respect to that of DPC and SC. Figs. 3a and 3b refer to differential attenuation. Once again, FSC shows an ability to remove any bias. In fact, the bias on the DPC estimates, perhaps due to considered DSDs that do not account for the used parameterizations, is totally negligible on FSC estimates. Although the performances of FSC and SC appears very close, NB and NSE of FSC present smaller values. Results for TEFLUN-B campaign (not shown) confirm these findings.

Attenuation correction procedure are validated in indirect way such as comparing rainfall estimates using corrected and uncorrected radar measurements with the ground true given by rain gauges or disdrometers. This technique introduces many additional sources of uncertainty that can make the comparison inadequate to validating. For this reason validation is also made using corrected radar data to establish

internal consistency among the polarimetric variables. Polar 55C data are here used to validate the FSC technique in an indirect way, based on statistical comparison of attenuation and differential attenuation estimates obtained with DPC and FSC, with respect the true values in the case of reconstructed C-band profiles. Under these conditions, fixing the tendency of the relative performances between DPC and FSC in order to verify if this trend is similar to that where the true values are unknown. Cumulative frequencies corresponding to the attenuation values estimated with DPC and FSC methods for the MAP and Polar 55C data sets are shown in Fig. 4a. For the MAP dataset, FSC presents the best performance because its cumulative frequency curve is superimposed to that of true attenuation. Polar 55C curves show a slower increase, due to the shorter pulse width. Comparing the relative differences in frequency between FSC and DPC estimated values for MAP and Polar 55C reveals the same trend – DPC increases less slowly than FSC. This allows us to think that the true attenuation frequency for the Polar 55C data set should be located as for the MAP case. The analysis on differential attenuation (Fig 4b) reveals a similar behavior, allowing to express the same conclusions also for the performance of FSC to estimate $\alpha_d$.

## 5 Conclusions

A methodology based on the self-consistency principle is proposed for the correction of attenuation and differential attenuation suffered by $Z_h$ and $Z_{dr}$ measurements. It is based on a procedure for attenuation correction at X-band (Gorgucci et al. 2006), optimized to make the procedure fully self-consistent, jointly using the quantities $Z_h$, $Z_{dr}$, $\Phi_{dp}$, $\alpha_h$ and $\alpha_d$ in a synergetic way. The technique is developed to obtain two scaling factors $\gamma_h$ and $\gamma_d$ to adjust $\alpha_h$ and $\alpha_d$, respectively. The solution optimizes for the best estimate of specific and cumulative attenuation as well as of specific and cumulative differential attenuation producing highly accurate estimates. The technique has been evaluated both using C-band radar profiles generated from S-band dual polarized measurements and C-band data collected by the Polar 55C radar. Evaluation shows the capability of FSC to remove any systematic bias that could arise from DSD and drop-shape variability along the path referred to the used parameterizations.

*Acknowledgements:* This research was partially supported by the the European Commission through the Interreg IIIB CADSES "RISK-AWARE" (3B064) project.

## References

Aydin K., Zhao Y., and T. A. Seliga, 1989: Rain-induced attenuation effects on C-band dual-polarization meteorological radars, *IEEE Trans. Geosci. Remote Sens.*, **27**, 57–66.

Bringi, V.N., V. Chandrasekar, N. Balakrishnan and D.S. Zrnić, 1990: An examination of propagation effects in rainfall on Radar measurements at microwave frequencies. *J. Atmos. and Oceanic Technol.,* **7**, 829–840.

Bringi V. N., Keenan T. D., and V. Chandrasekar, 2001: Correcting C-band radar reflectivity and differential reflectivity data for rain attenuation: a self-consistent method with constraints, *IEEE Trans. Geosci. Remote Sens.*, **39**, 1906–1915.

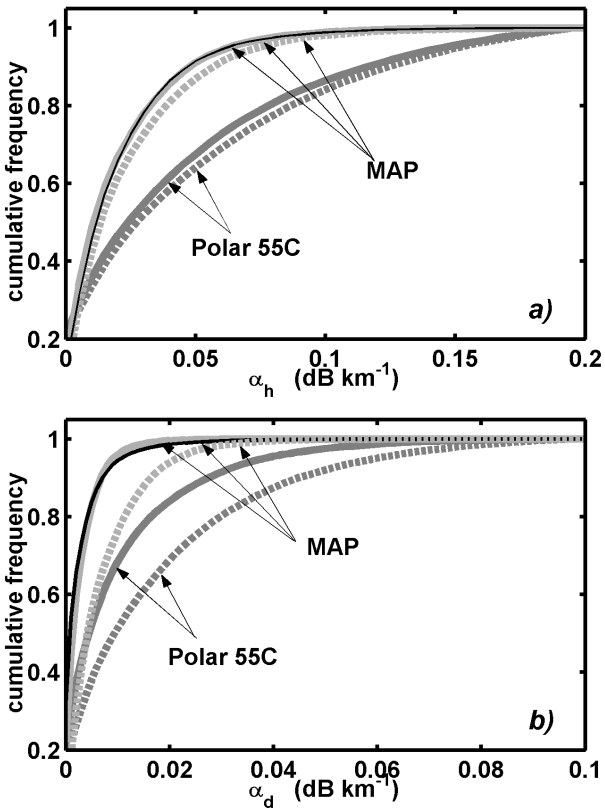


**Fig. 4.** – Cumulative frequencies of a) specific attenuation b) specific differential attenuation estimates for MAP (light grey) and Polar 55C (dark grey) data using DPC (dash) and FSC (solid) methods. Black curve is the cumulative frequencies of the true specific attenuation for MAP.

Chandrasekar V., Lim S., and E. Gorgucci, 2006: Simulation of X-band rainfall observations from S-band radar data *J. Atmos. Oceanic Technol*. (in print).

Gorgucci, E., Scarchilli, G., Chandrasekar, V., Meischner, P. F., and M. Hagen, 1988: Intercomparison of techniques to correct for attenuation of C-band weather radar signals, *J. Appl. Meteor*., **37**, 845–853.

Gorgucci, E., Scarchilli, G., Chandrasekar, V., 2000: Practical aspects of radar rainfall estimation using specific differential propagation phase. J. Appl. Meteor., **39**, 945–955, 2000.

Gorgucci E., Baldini L., and A. Volpi, 2002: Polar 55C: an upgraded instrument for polarimetric radar research, Proc. of the 2nd European Conf. on Radar Meteorol. ERAD, Delft, The Netherlands, 394-399.

Gorgucci, E. Chandrasekar V., and L. Baldini, 2006: Correction of X-band radar observation for propagation effects based on the self-consistency principle, *J. Atmos. Oceanic Technol.*, (in print).

Pruppacher, H. R. and K.V. Beard, 1970: A wind tunnel investigation of the internal circulation and shape of water drops falling at terminal velocity in air. *Quart. J. Roy. Meteor. Soc.*, **96**, 247-256.

Scarchilli G., E. Gorgucci, V. Chandrasekar, and A. Dobaie, 1996: Self-consistency of polarization diversity measurement of rainfall. *IEEE Trans. Geosci. Remote Sens.,* **34,** 22–26.

Smyth, T. J., and A. J. Illingworth, 1998: Correction for attenuation of radar reflectivity using polarization data. *Quart. J. Roy. Meteor. Soc.*, **124**, 2393-2415.

Testud, J., E. Le Bouar, E. Obligis, and M. Ali-Mehenni, 2000: The rain profiling algorithm applied to polarimetric weather radar. *J. Atmos. Oceanic Technol.,* **17,** 332–356.